Supplementary Material (ESI) for Lab on a Chip

Supplementary Information

Dynamic pH mapping in microfluidic devices by integrating adaptive coatings based on polyaniline with colorimetric imaging techniques

Larisa Florea[1], Cormac Fay[1], Emer Lahiff[1], Thomas Phelan[1], Noel E. O'Connor[1], Brian Corcoran[1], Dermot Diamond[1] and Fernando Benito-Lopez[1,2]*

[1]*CLARITY: Centre for Sensor Web Technologies, National Centre for Sensor Research, Dublin City University, Dublin, Ireland*

[2]*CIC MicroGUNE, Microtechnologies Cooperative Research Center, Arrasate-Mondragón, Spain*

* *To whom correspondence should be addressed. Tel.: +34 943710212 Fax: +34943710212; E-mail: fbenito@cicmicrogune.es or fernando.lopez@dcu.ie*

Table of Contents

Section 1: Materials and methods

Aniline (BDH), HCl (Fisher Scientific), ammonium persulfate (Aldrich), *N*-[3-(Trimethoxylsilyl)propyl]aniline (Aldrich), sodium hydroxide (Aldrich) were used. The aniline monomer was purified by vacuum distillation before use. Other chemicals were used as received.

Raman Spectroscopy was employed to study the chemical features of the polyaniline coatings inside the microchannel. Raman spectra were taken with a Perkin Elmer RamanStation at 2 cm^{-1} resolution, 3s per scan and 10–20 collections. A 785 nm laser line was used as it can detect both doped and dedoped features in polyaniline.

Scanning Electron Microscopy (SEM) was carried out at an accelerating voltage of 20kV on a S-4300 Hitachi system. For imaging purposes the PDMS layer of the PDMS/glass microchannel was removed. The glass layer containing the polyaniline film was coated with 10 nm Au prior to imaging.

UV-Vis Spectroscopy was used to study the pH dependence of the polyaniline coatings. The absorbance spectra were recorded using 2 fiber-optic light guides connected to a Miniature Fiber Optic Spectrometer (USB4000 - Ocean Optics) and aligned using an in-house made cell (see Figure S1). The light source used was a Deuterium – Halogen light source (Top Sensor Systems).

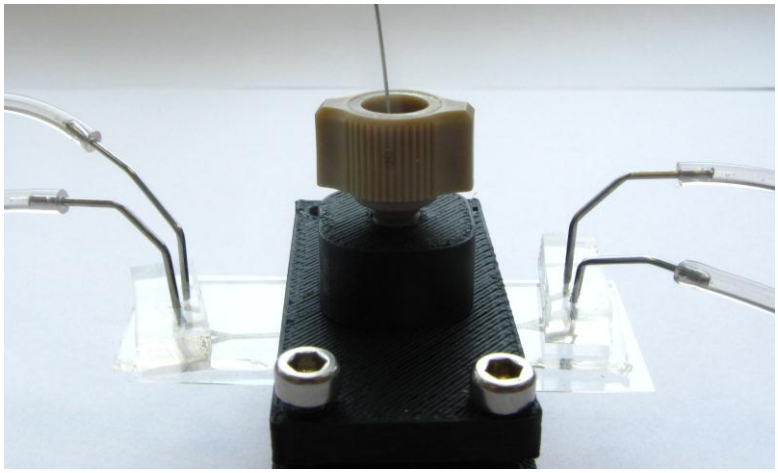

Figure S1. *In house designed holder used for absorbance measurements of the PAni coatings.*

Section 2: Digital image capture

Throughout the calibration routine, the images were captured using a Panasonic DMC-FZ38 digital colour camera which was held in a fixed position via a retort stand at a distance of 7 cm from the microchannel / reference chart to fully capture the image scene, see Figure S3. The camera was set to capture in RAW format to eliminate possible image artefacts and at a resolution of 4016x 3016 (12 MPixels). The other camera settings were as follows: F-Number (2.8), Max aperture (F2.8), No Flash and a Focal Length of 4.8 mm.

Once the images were captured, they underwent a segmentation process where pixels representing the flow channel and reference patches were identified and separated into image regions. This was achieved through the use of an Interactive Segmentation Toolkit[9]. Although an unsupervised/automatic segmentation algorithm was possible, it was felt that this supervised approach was more robust to misclassifications and as a result, it fully ensured the location and determination of the reference patches and channel regions. A binary mask image resulted from this process with black pixels representing areas of non interest (*e.g.* the background) and white regions representing the reference colour patches and the flow channel. Finally, a binary erosion algorithm was applied to remove possible boundary pixels and also any isolated white pixels *i.e.* to ensure robustness for subsequent processing steps, see Figure S3.

(a) (b)

Figure S2. *Picture of a captured image (a) during the experimental procedure showing the colour reference chart/patches and flow channel. Mask image (b) after image processing algorithms are applied.*

Next, it was necessary to identify each region separately for correct analysis. Therefore, a connected component analysis step was applied to the binary mask image which assigned a unique region identification number to each image area with connected white pixels. This allowed for each of the reference patches and flow channel to be analysed separately at a later stage. Subsequently, due to the consistency across all images (from the experimental constraints) it was possible to easily identify each region based on their spatial coordinates within the image. As a result, each patch was identified correctly in all instances via their calculated centroid locations in each subsequent image.

After that, the calibration images were taken and processed. Initially, the original images underwent a white balance process in order to compensate for possible changes in the ambient lighting environment. This involved generation of the histograms for each of the Red, Green and Blue channels of the captured sRGB colour space. Next, a bin threshold was determined at either end of each histogram. Pixel counts that used less than 0.05% of the total image pixels were discarded at each histogram ends and the histograms were stretched to the boundary i.e. 0 and 255. The images were then reconstructed. Next, a copy of this image was made and transformed from the captured sRGB colour space into the HSV (Hue, Saturation and Value) colour space[10]. Following this, the binary mask image was applied to the HSV image through a simple pixel-by-pixel binary AND operation on the Hue channel alone. Finally, the colour of each region was ascertained by calculating its Hue average and saving it to an external file in CSV (comma separated value) format for all regions within each image for later analysis.

The gradient analysis step took place in much the same way as with the calibration image processing. However, instead of calculating the Hue average over the entire flow channel region, a localised average was considered at discrete points along the channel's path. This was achieved by firstly isolating the flow channel region alone via its bounding box and using that to crop the image thereby removing the reference patches. Here, a medial axis transformation was applied to this singular binary region resulting in an 8-connected contour line alone the centre of the channel at a width of 1 pixel[11], see Figure S4. After this, the starting point was identified to be at the most extreme upper left white pixel of the contour. Next, a binary circular mask image with a diameter of 35 pixels was created and combined (binary AND

operation) with the binary mask image of the channel at the starting point. The resulting mask was, in turn, applied to the Hue channel at the same location. Finally, the average Hue value at this sub region was calculated and saved to a CSV file. The process was repeated at every pixel location along the contour with all values saved to file.

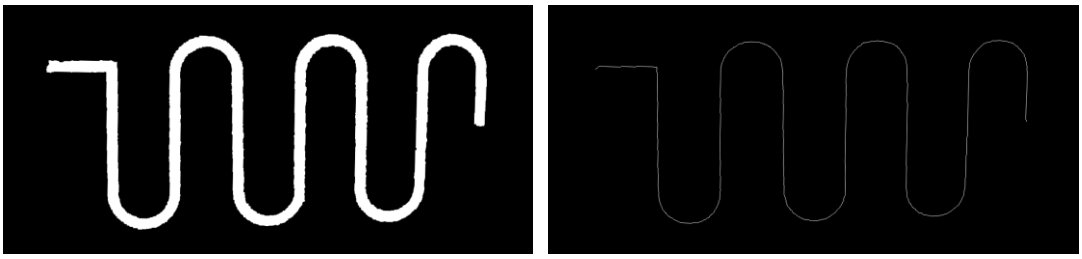

Figure S3*. Processed images showing the mask region of the flow channel (left) and the result of applying a medial axis transformation (right).*

Section 3: Characterisation of polyaniline (PAni) coating by Raman Spectroscopy

Raman spectroscopy is a very powerful technique for the analysis of intrinsically conducting polymers. Here, Raman spectroscopy is employed to study the chemical structure of the coating as this technique permits in situ analysis of the polyaniline coating inside the microchannel. In the case of polyaniline, Raman spectroscopy can also be used to study its doping-dedoping behaviour as very distinct signature bands appear for the quinoid and benzenoid rings respectively.

Figure S2 presents the Raman spectra of a polyaniline functionalised microchannel taken after a solution of pH 2 (HCl, 10^{-2} M) and pH 12 (NaOH, 10^{-2} M), respectively are passed inside the microchannel. For comparison, the spectrum of a bare PDMS microchannel is also shown (black). For low pH values the polymer exists in the doped state, emeraldine salt (ES). Increasing the pH causes a change in the bonding structure of the material, and at high pH values PAni is present in its dedoped state – emeraldine base (EB). Signature bands between 1300 and 1400 cm^{-1} appear for the doped material (Fig. S2 – in green). These are less significant at higher pH values, and strong bands between 1400 and 1500 cm^{-1} reflect the dedoped state (Fig. S2 – in blue).

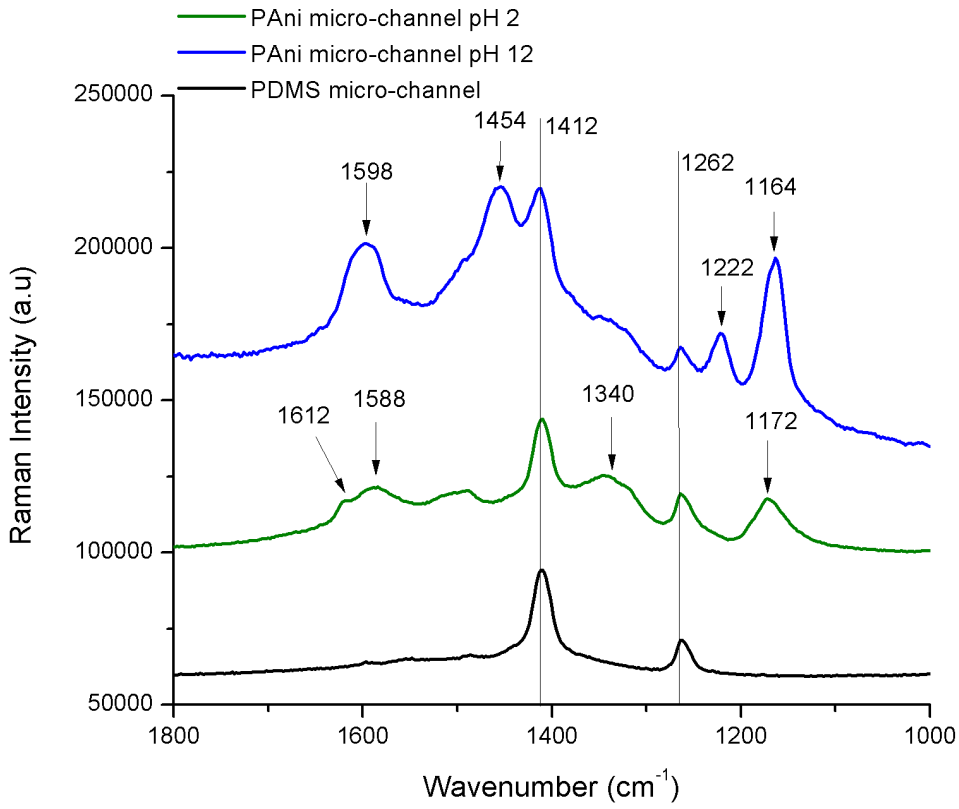

Figure S4. *Raman Spectra of unfunctionalised PDMS microchannel (black), PAni functionalised microchannel after being filled with a pH2 HCl solution (green) and PAni functionalised microchannel after being filled with a pH12 NaOH solution (blue).*

In particular, in the case of EB, an important peak can be observed at 1454 cm^{-1} and is characteristic to C=N stretching vibration of the quinoid units[1-5]. Other bands at 1596 cm^{-1} and 1164 cm^{-1}, are assigned to C-C stretching[1, 4] and C-H bending modes[1, 2], respectively, centered on the quinoid ring. Another new peak at 1221 cm^{-1} appears in the spectra of polyaniline upon dedoping and is assigned to C–N stretching vibrations of the benzenoid units [1, 4] (the EB form consists of both C=N and C-N bonds). In the case of ES, the most important band appears at 1340 cm^{-1} and can be assigned to a C-N• + polaron stretch [1, 4, 6, 7] while the band at 1172 cm^{-1} is characteristic to the C–H in-plane bending of the benzenoid ring [1, 5]. Both C - C stretching vibrational modes, in the benzenoid and quinoid rings, are seen at 1612 cm^{-1} and 1588 cm^{-1}, respectively [4], in the case of polyaniline spectra taken at pH 2. This suggests that minor fractions of non protonated quinoid rings are still present in the structure. It has been shown before that the Raman Intensity is enhanced in the

case of EB compared with ES when a 785 nm laser is used [5]. The PAni coating may also be partially excited to the EB form by the incoming laser radiation resulting in resonant enhancement of the lines originating from the quinoid ring [4]. The specific vibrations of PDMS can also be found in the spectra of polyaniline coatings since polyaniline is attached to the inner walls of the PDMS/ glass microchannel. The CH_3 bending vibrations appear at 1263 cm^{-1} and 1412 cm^{-1} [8]. Other bands specific to the PDMS layer are also present: Si-O-Si symmetric stretching (490 cm^{-1}), Si-C symmetric stretching (708 cm^{-1}), CH3 symmetric stretching (2904 cm^{-1}), and CH3 asymmetric stretching (2964 cm^{-1})[8], but not shown here.

Section 4: pH measurements

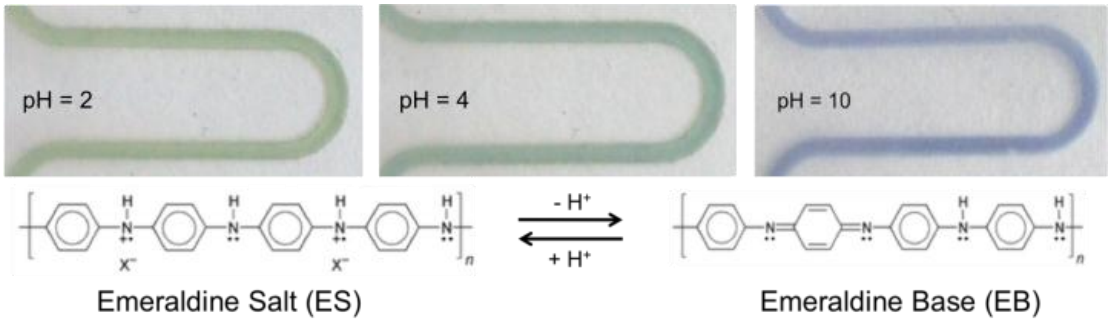

Figure S5*. Photos of a microchannel loop when solutions of different pHs are flushed through the channel. The photos are accompanied by a scheme showing the differences in the chemical structure of polyaniline (two different states: Emeraldine Salt and Emeraldine Base).*

Section 5: pH determination via colorimetric imaging analysis

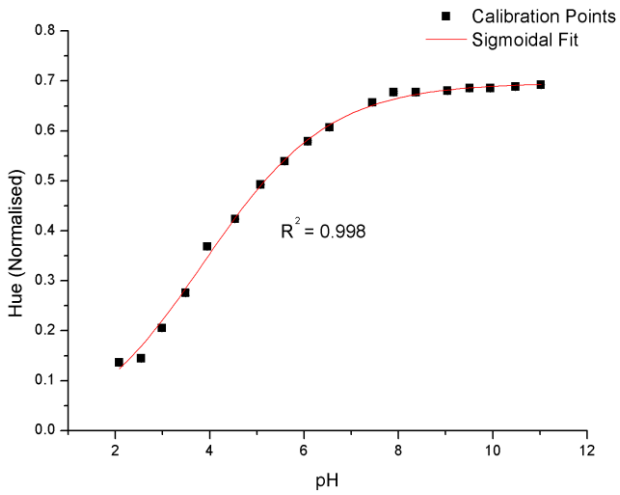

Figure S6*. Calibration plot of the camera and channel to changing pH. Points represent the normalised average Hue value of the channel's colour across multiple images and the error bars (occluded by the points) represent their standard deviation. The line is a sigmoidal fit after applying Boltzmann's regression technique (R^2 = 0.998, n = 18).*

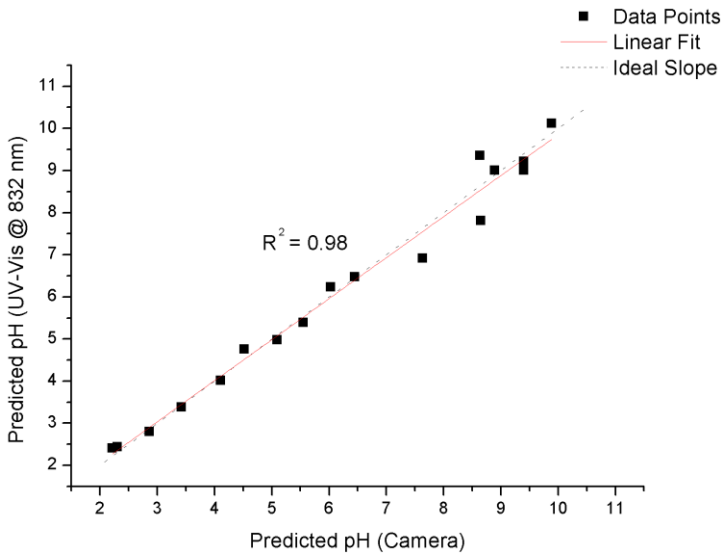

Figure S7. *Plot showing the correlation between predicted pH using the camera and UV-Vis at 832 nm. The line represents a linear fit (R^2 = 0.98, n = 18).*

Section 6: References

1. K. Berrada, S. Quillard, G. Louarn and S. Lefrant, Synth. Met. **69** (1-3), 201-204 (1995).
2. Y. Furukawa, T. Hara, Y. Hyodo and I. Harada, Synth. Met. **16** (2), 189-198 (1986).
3. A. Hugotlegoff and M. C. Bernard, Synth. Met. **60** (2), 115-131 (1993).
4. J. Laska, R. Girault, S. Quillard, G. Louarn, A. Pron and S. Lefrant, Synth. Met. **75** (1), 69-74 (1995).
5. T. Lindfors and A. Ivaska, J. Electroanal. Chem. **580** (2), 320-329 (2005).
6. C. Liu, J. X. Zhang, G. Q. Shi and F. E. Chen, J. Appl. Polym. Sci. **92** (1), 171-177 (2004).
7. R. Mazeikiene, A. Statino, Z. Kuodis, G. Niaura and A. Malinauskas, Electrochem. Commun. **8** (7), 1082-1086 (2006).
8. S. C. Bae, H. Lee, Z. Q. Lin and S. Granick, Langmuir **21** (13), 5685-5688 (2005).
9. K. McGuinness and N. E. O'Connor, Pattern Recognition **43** (2), 434-444 (2010).
10. A. R. Smith, SIGGRAPH Comput. Graph. **12** (3), 12-19 (1978).
11. T. Y. Zhang and C. Y. Suen, Communications of the Acm **27** (3), 236-239 (1984).